Published in final edited form as:
Cancer Res. 2009 September 1; 69(17): 6932–6940. doi:10.1158/0008-5472.CAN-09-1682.

Preclinical Evaluation of Novel Glutamate-Urea-Lysine Analogs that Target Prostate Specific Membrane Antigen as Molecular Imaging Pharmaceuticals for Prostate Cancer

Shawn M. Hillier[1], **Kevin P. Maresca**[1], **Frank J. Femia**[1], **John C. Marquis**[1], **Catherine A. Foss**[2], **Nghi Nguyen**[1], **Craig N. Zimmerman**[1], **John A. Barrett**[1], **William C. Eckelman**[1], **Martin G. Pomper**[2], **John L. Joyal**[1], and **John W. Babich**[1]

[1]Molecular Insight Pharmaceuticals, Cambridge, MA, USA

[2]Department of Radiology, Johns Hopkins Medical Institutions, Baltimore, MD, USA

Abstract

Prostate-specific membrane antigen (PSMA) is expressed in normal human prostate epithelium and is highly upregulated in prostate cancer. We previously reported a series of novel small molecule inhibitors targeting PSMA. Two compounds, MIP-1072, (*S*)-2-(3-((*S*)-1-carboxy-5-(4–iodobenzylamino)pentyl)ureido)pentanedioic acid and MIP-1095, (*S*)-2-(3-((*S*)-1-carboxy-5-(3-(4-iodophenyl)ureido)pentyl)ureido)pentanedioic acid, were selected for further evaluation. MIP-1072 and MIP-1095 potently inhibited the glutamate carboxypeptidase activity of PSMA (K_i = 4.6 ± 1.6 and 0.24 ± 0.14 nM, respectively), and when radiolabeled with ^{123}I exhibited high affinity for PSMA on human prostate cancer LNCaP cells (K_d = 3.8 ± 1.3 and 0.81 ± 0.39 nM, respectively). The association of [^{123}I]MIP-1072 and [^{123}I]MIP-1095 with PSMA was specific; there was no binding to human prostate cancer PC3 cells, which lack PSMA, and binding was abolished by co-incubation with a structurally unrelated NAALADase inhibitor, 2-(phosphonomethyl)pentanedioic acid (PMPA). [^{123}I]MIP-1072 and [^{123}I]MIP-1095 internalized into LNCaP cells at 37 °C. Tissue distribution studies in mice demonstrated 17.3 ± 6.3 (at 1 hr) and 34.3 ± 12.7 (at 4 hr) % injected dose per gram of tissue, for [^{123}I]MIP-1072 and [^{123}I]MIP-1095, respectively. [^{123}I]MIP-1095 exhibited greater tumor uptake but slower washout from blood and non-target tissues compared to [^{123}I]MIP-1072. Specific binding to PSMA *in vivo* was demonstrated by competition with PMPA in LNCaP xenografts, and the absence of uptake in PC3 xenografts. The uptake of [^{123}I]MIP-1072 and [^{123}I]MIP-1095 in tumor bearing mice was corroborated by SPECT/CT imaging. PSMA-specific radiopharmaceuticals should provide a novel molecular targeting option for the detection and staging of prostate cancer.

Corresponding Author: John W. Babich, Molecular Insight Pharmaceuticals, 160 Second Street, Cambridge, MA, USA, jbabich@molecularinsight.com, Telephone: 617-492-5554, Fax: 617-492-5664.

Disclosure of potential conflicts of interest

This work was conducted at Molecular Insight Pharmaceuticals, Inc. S. Hillier, K. Maresca, F. Femia, J. Marquis, C. Zimmerman, J. Barrett, J. Joyal, and J. Babich are employees of Molecular Insight Pharmaceuticals, Inc. W. Eckelman and M. Pomper are consultants for Molecular Insight Pharmaceuticals, Inc.

Keywords

prostate cancer; molecular imaging; prostate-specific membrane antigen; NAALADase; SPECT

Introduction

Prostate cancer is the most commonly diagnosed malignancy and the second leading cause of cancer related deaths in men in the United States (1). In 2009, it is estimated that 192,000 men will be diagnosed with prostate cancer and 27,000 men will die of the disease (1). Current diagnosis is typically through digital rectal exam (DRE) and blood prostate specific antigen (PSA) testing. Since the introduction of serum PSA screening, prostate cancer incidence rates have increased dramatically as have the number of men being treated for the disease (2). However, 20–30% of men with prostate cancer have serum PSA levels within the normal range, resulting in false negatives (3,4), while others have elevated serum PSA levels due to conditions other than prostate cancer (i.e., benign prostatic hyperplasia), resulting in false positives and unnecessary biopsies (5). Since elevated serum PSA levels do not always correlate with disease, there is skepticism regarding the value of broad-based PSA testing with regard to predicting surgical cures (6). Initial results from the Prostate, Lung, Colorectal and Ovarian (PLCO) Cancer Screening Trial showed that annual PSA testing for 6 years and annual DRE testing for 4 years (performed in the same years as the first four PSA tests) did not reduce the number of deaths from prostate cancer through a median follow-up period of 11.5 years. These results suggest that many men were diagnosed with, and treated for, cancers that would not have been detected in their lifetime without screening and, as a consequence, were exposed to the potential harms of unnecessary treatments, such as surgery and radiation therapy (7). Therefore, accurate initial diagnosis and determination of the extent of disease continues to be a major challenge for selecting appropriate treatment options, monitoring the effects of therapeutic interventions, and detecting disease after recurrence. New agents that will more accurately diagnose and stage prostate cancer, as well as monitor therapy, will enable improved treatment planning and result in improved patient outcome.

Prostate-specific membrane antigen (PSMA), also known as folate hydrolase I (FOLH1) or glutamate carboxypeptidase II (GCPII), is a transmembrane, 750 amino acid, type II glycoprotein that is primarily expressed in normal human prostate epithelium but is overexpressed in prostate cancer, including metastatic disease (8–10). PSMA is an *N*-acetylated-alpha-linked acidic dipeptidase (NAALADase) with reactivity toward poly-gamma-glutamyl folates and has the capability of sequentially removing the poly-gamma-glutamyl termini of dipeptides (11,12). Since PSMA is expressed by virtually all prostate cancers and its expression is further increased in poorly differentiated, metastatic and hormone-refractory carcinomas (9), it is a very attractive target for prostate cancer imaging and therapy.

PSMA was originally identified as the ligand of the monoclonal antibody 7E11-C5, marketed as ProstaScint™ (Capromab Pendetide), with a histological profile that demonstrated a high degree of specificity for the LNCaP human adenocarcinoma cell line

(10). ProstaScint™ is not in widespread use in part because it targets the intracellular domain of PSMA (amino terminus) and is believed to bind mostly necrotic portions of prostate tumors and not to viable tumor cells (13,14). More recently, radiolabeled monoclonal antibodies have been developed that bind to the extracellular domain of PSMA and have been shown to accumulate in PSMA-positive prostate tumor models in animals (15). Early promising results from clinical trials have demonstrated the utility of PSMA as a diagnostic and therapeutic target (16,17). While monoclonal antibodies hold promise for tumor detection and therapy, there have been limited clinical successes outside of lymphoma because of their long circulating plasma half-lives and low permeability in solid tumors, particularly in metastases to the bone. Lower molecular weight small molecules, with higher permeability in solid tumors, will likely have an advantage. In addition, small molecules will likely display improved pharmacokinetics in normal tissues as compared with intact immunoglobulins, making lesion detection more conspicuous.

Recently, Maresca et al, described the design and synthesis of a series of small molecule inhibitors of PSMA (18), with the potential to diagnose and stage prostate cancers through commonly used molecular imaging modalities such as single photon emission computed tomography (SPECT). Here we evaluate two of the most potent radioiodinated compounds, [^{123}I]MIP-1072 and [^{123}I]MIP-1095, for their ability to bind to PSMA and localize to PSMA expressing tumors *in vivo*.

Materials and Methods

Synthesis and radiolabeling of MIP-1072 and MIP-1095

The synthesis of MIP-1072 (*S*)-2-(3-((*S*)-1-carboxy-5-(4–iodobenzylamino)pentyl)ureido)pentanedioic acid and MIP-1095 (*S*)-2-(3-((*S*)-1-carboxy-5-(3-(4-iodophenyl)ureido)pentyl)ureido)pentanedioic acid, along with the radiolabeling precursors trimethyltin-MIP-1072 and trimethyltin-MIP-1095, and their subsequent radiolabeling with ^{123}I were described previously (18). Briefly, radiolabeling was accomplished by iododestannylation of the trimethylstannyl precursors (*S*)-di-*tert*-butyl 2-(3-((*S*)-1-*tert*-butoxy-1-oxo-6-(4–(trimethylstannyl)benzylamino)hexan-2-yl)ureido)pentanedioate and (*S*)-di-*tert*-butyl 2-(3-((*S*)-1-*tert*-butoxy-1-oxo-6-(3-(4-(trimethylstannyl)phenyl)ureido)hexan-2-yl)ureido)pentanedioate with 50–100 mCi of [^{123}I]NaI employing acidic oxidizing conditions to form [^{123}I]MIP-1072 and [^{123}I]MIP-1095, respectively, in moderate radiochemical yields (50–70%) in as little as 10 minutes. The radioiododestannylation afforded the ^{123}I labeled tri-*tert*-butyl esters which were purified using simple C18 Sep Pak columns and deprotected with TFA to afford the desired radioiodinated inhibitors in >95% radiochemical purity. The specific activity was determined to be ≥ 4000 Ci /mmol.

NAALADase Inhibition by MIP-1072 and MIP-1095

The ability of non-radiolabeled MIP-1072 and MIP-1095 to inhibit the NAALADase activity of PSMA was tested in LNCaP cell lysates as previously described (19) with minor modifications. Briefly, LNCaP cells were collected, washed in 0.32 M sucrose, and lysed in cold 50 mM Tris-HCl, pH 7.4, 0.5% Triton X-100. The lysate was centrifuged at 20,000 X g

to remove insoluble material, then aliquoted and stored frozen at -80 °C. LNCaP cell lysate (100 μg) was added to 10 μM ^{3}H-*N*-acetylaspartylglutamate (^{3}H-NAAG) (Perkin Elmer, Waltham, MA) in 50mM Tris-HCl pH 7.4, 20 mM $CoCl_2$, 32 mM NaCl in the presence of 1–10,000 nM test compounds. After 30 minutes, the reaction was stopped by adding an equal volume of cold 0.25 M KH_2PO_4. The assay mixture was applied to an AG 50W-X4 cation exchange column (200–400 mesh, H^+ form) (Bio-Rad Laboratories, Hercules, CA), and eluted with 3 M KCl. Eluates were counted for determination of the amount of ^{3}H-glutamate liberated. Inhibitory constants (K_i) were calculated from the IC_{50} values using the Cheng-Prusoff equation (20).

Cell Culture

Human prostate cancer cell lines, LNCaP (PSMA positive) and PC3 (PSMA negative), were obtained from the American Type Culture Collection (Rockville, MD). PC3 cells transfected with either PSMA (PC3 PIP) or plasmid alone (PC3 flu) were obtained from Dr. Warren Heston (Cleveland Clinic, Cleveland, OH) and maintained as previously described (21). LNCaP cells were maintained in RPMI-1640 medium (Invitrogen, Carlsbad, CA) supplemented with 10% fetal bovine serum (Hyclone, Logan, UT) in a humidified incubator at 37 °C/5% CO_2. PC3 cells were maintained in F12K Nutrient Mixture Kaighn's Modification Medium (Invitrogen, Carlsbad, CA) supplemented with 10% fetal bovine serum in a humidified incubator at 37 °C/5% CO_2. Cells were removed from flasks for passage or for transfer to 12-well assay plates by incubating them with 0.25% trypsin/EDTA (Invitrogen, Carlsbad, CA).

Direct Binding

LNCaP cells and PC3 cells (3×10^5 cells/well in 12-well plates in duplicate) were incubated in RPMI-1640 medium supplemented with 0.5% bovine serum albumin for 1 hour at room temperature with 3 nM [^{123}I]MIP-1072 or [^{123}I]MIP-1095 alone, or in the presence of 10 μM non-radiolabeled iodinated test compound, or 10 μM 2-(phosphonomethyl)-pentanedioic acid (PMPA) (Axxora, San Diego, CA), a structurally unrelated NAALADase inhibitor. Cells were washed and counted in an LKB Wallac Model 1282 automated gamma counter (Perkin Elmer, Waltham, MA).

Saturation Binding

The affinity constant (K_d) of MIP-1072 and MIP-1095 was determined by saturation binding analysis. LNCaP cells (3×10^5 cells/well in 12-well plates in triplicate) were incubated for 1 hour with 30–300,000 pM [^{123}I]MIP-1072 or [^{123}I]MIP-1095 in HBS (50 mM Hepes, pH 7.5, 0.9% sodium chloride) at 4 °C. Nonspecific binding was determined by adding 10 μM non-radiolabeled MIP-1072 or MIP-1095. Cells were then washed and the amount of radioactivity was measured on a gamma counter. Specific binding was calculated as the difference between total binding and nonspecific binding. The K_d and B_{max} were determined by nonlinear regression analysis using GraphPad Prism (La Jolla, CA) software.

Internalization

LNCaP cells (3×10^5 cells/well in 12-well plates in duplicates) were incubated in HBS with 100 nM [^{123}I]MIP-1072 or [^{123}I]MIP-1095 for 0–2 hours at 4 and 37 °C. At the indicated time the media was removed and the cells were washed with a mild acid buffer (50 mM glycine, 150 mM NaCl, pH 3.0) at 4 °C for 5 minutes. Cells were then centrifuged at 20,000 × *g* for 5 minutes. The supernatant (containing cell surface bound radioactivity) and the cell pellet (containing internalized radioactivity) were counted on a gamma counter (22).

Inoculation of Mice with Xenografts

All animal studies were approved by the Institute for Animal Care and Use Committee in accordance with the guidelines set forth by the U.S. Public Health Service *Policy on Humane Care and Use of Laboratory Animals*. Mice were housed under standard conditions in approved facilities with 12 hour light/dark cycles and given food and water *ad libitum.* Male athymic NCr-nu/nu mice were purchased from Taconic (Hudson, NY). Mice were anesthetized by an intraperitoneal injection of approximately 0.5 mL/mouse avertin (19 mg/ml). For inoculation in mice, LNCaP or PC3 cells were resuspended at 10^7 cells/ml in a 1:1 mixture of cell culture medium:Matrigel (BD Biosciences, Franklin Lakes, NJ). Each mouse was injected in the right flank with 0.25 ml of the cell suspension. Mice were used for tissue distribution studies when the tumors reached approximately 100–400 mm^3. Male severe combined immunodeficient mice (Charles River Laboratories, Wilmington, MA) were implanted with $1–5\times10^6$ cells suspended in HBSS (Sigma-Aldrich, St. Louis, MO) behind the left shoulder (PC3 PIP) and right shoulder (PC3 flu).

Mouse Tissue Distribution

A quantitative analysis of the tissue distribution of [^{123}I]MIP-1072, [^{123}I]MIP-1095, or ProstaScint™ (Cardinal Health, Dublin, OH) was performed in separate groups of male NCr-nu/nu mice bearing LNCaP or PC3 cell xenografts administered via the tail vein as a bolus injection (approximately 2 μCi/mouse at a specific activity of >1000 mCi/μmol) in a constant volume of 0.05 mL. The animals (n=5/time point) were euthanized by asphyxiation with carbon dioxide at 0.25, 1, 2, 4, 8, and 24 hours after injection. To examine specificity, other mice (n=5) were co-injected with 50 mg/kg PMPA and sacrificed at 2 hours. Tissues were dissected, excised, weighed wet, and counted in an automated γ-counter. Tissue time-radioactivity levels expressed as percent injected dose per gram of tissue (%ID/g) were determined.

SPECT/CT Imaging

All *in vivo* experimental procedures were undertaken in compliance with United States laws governing animal experimentation and were approved by the Johns Hopkins University IACUC. Male Fox Chase SCID mice were each implanted with either 5×10^6 LNCaP cells, or, 5×10^6 PC-3 PIP (PSMA+) and PC-3 flu (PSMA-) cells on opposite flanks. When the tumors reached approximately 5–7 mm in diameter, mice were anesthetized using 1% isoflurane gas in oxygen flowing at 0.6 L/min prior to and during radiopharmaceutical injection. Mice were injected *via* the tail vein with 1 mCi of either [^{123}I]MIP-1072 or [^{123}I]MIP-1095 at a specific activity of >1000 mCi/μmol. Mice bearing LNCaP tumors were

imaged 4 hr post-injection and mice bearing PC-3 PIP or flu tumors were imaged at 2 hr post-injection. A Gamma Medica (Northridge, CA) X-SPECT scanner equipped with two opposing low-energy 0.5 mm aperture pinholes and tunable CT was used for all scans. Mice were scanned over 180° in 5.5°, 45 second increments. A CT scan was performed prior to scintigraphy for both anatomical coregistration and attenuation correction. Data were reconstructed and fused using commercial software from the vendor (Gamma Medica), which includes a 2D-OSEM algorithm.

Results

MIP-1072 and MIP-1095 are potent inhibitors of NAALADase

The ability of MIP-1072 and MIP-1095 to inhibit the glutamate carboxypeptidase activity of PSMA was tested in LNCaP cellular lysates by monitoring the hydrolysis of ^{3}H-NAAG. The K_i values for MIP-1072 and MIP-1095 were 4.6 ± 1.6 and 0.24 ± 0.14 nM, respectively, indicating that both MIP-1072 and MIP-1095 are potent inhibitors of NAALADase enzymatic activity. The greater potency of MIP-1095 compared to MIP-1072 is consistent with competitive binding data (18). The structurally unrelated PSMA inhibitor, PMPA, was included as a positive control and displayed a K_i of 2.1 ± 0.1 nM, in agreement with the K_i determined by Tiffany, et al (23).

[^{123}I]MIP-1072 and [^{123}I]MIP-1095 bind to cells expressing PSMA and are internalized

LNCaP and PC3 cells were incubated with [^{123}I]MIP-1072 or [^{123}I]MIP-1095 to examine the specificity for PSMA expressing prostate cancer cells. Both compounds bound to LNCaP cells but not to the PSMA deficient PC3 cells. Binding to LNCaP cells was inhibited by either non-radiolabeled compound or the structurally unrelated PSMA inhibitor, PMPA (Figure 1A).

Saturation binding analysis was conducted to determine the affinity of [^{123}I]MIP-1072 and [^{123}I]MIP-1095 for PSMA expressed on LNCaP cells. Cells were incubated with 30–300,000 pM [^{123}I]MIP-1072 or [^{123}I]MIP-1095 to determine K_d and B_{max} (Figure 1B). Consistent with the order of potency of the NAALADase inhibition assay, MIP-1095 was found to have greater affinity for PSMA than MIP-1072 (K_d = 0.81 ± 0.39 and 3.8 ±1.3 nM, respectively). The B_{max} obtained with MIP-1072 was found to be 1490 ± 60 fmol/10^6 cells (0.9×10^6 sites/cell) and the B_{max} obtained with MIP-1095 was found to be 1680 ± 110 fmol/10^6 cells (1×10^6 sites/cell), consistent with the value obtained with the ProstaScint™ antibody (12).

To determine if [^{123}I]MIP-1072 and [^{123}I]MIP-1095 are internalized into LNCaP cells by endocytosis, cells were incubated with [^{123}I]MIP-1072 or [^{123}I]MIP-1095 for up to 2 hr at 4 and 37 °C, and washed with a mild acid buffer to remove compound that is bound to the cell surface. Figure 1C depicts the total binding (dashed lines) of [^{123}I]MIP-1072 and [^{123}I]MIP-1095 and the acid insensitive binding, or internalized compound, (solid lines) to LNCaP cells. The results show a time dependent increase in radioactivity associated with the cellular pellet at 37 °C but not at 4 °C, indicating internalization in a temperature dependent manner. These results were confirmed by a saturation binding analysis at 37 °C which

showed an elevation in the apparent B_{max} of both compounds, indicating internalization (data not shown).

[^{123}I]MIP-1072 and [^{123}I]MIP-1095 localize to PSMA expressing tissues *in vivo*

The tissue distribution of [^{123}I]MIP-1072 and [^{123}I]MIP-1095 was assessed in NCr-nu/nu mice bearing LNCaP xenografts and the results are illustrated in Table 1. The radiolabel was detected at varying levels in all tissues examined and generally decreased over time. At 24 hr blood and non-target tissues were at or below the limits of detection in mice injected with [^{123}I]MIP-1072 or [^{123}I]MIP-1095. As anticipated, [^{123}I]MIP-1072 and [^{123}I]MIP-1095 uptake and exposure was greatest in the kidney, which has been shown to express high levels of NAALADase (9), and in PSMA positive LNCaP xenografts. Peak kidney accumulation for [^{123}I]MIP-1072 was 159 ± 46 %ID/g at 2 hr and peak LNCaP xenograft accumulation was 17.4 ± 6.3 %ID/g at 1 hr. Peak kidney accumulation for [^{123}I]MIP-1095 was 88.7 ± 23.8 %ID/g at 2 hr and peak LNCaP xenograft accumulation was 34.3 ± 12.7 %ID/g at 4 hr. Clearance from the LNCaP xenograft between 1 and 24 hours was slower with [^{123}I]MIP-1095 than with [^{123}I]MIP-1072 ($P < 0.05$). There was no significant difference in the level of [^{123}I]MIP-1095 in the LNCaP xenograft between 1 and 24 hours ($P > 0.06$). [^{123}I]MIP-1095 demonstrated a slower clearance from blood and most organs compared to [^{123}I]MIP-1072 ($P < 0.05$ for blood, heart, lungs, liver, spleen, kidneys, stomach, intestines, and testes between 1 and 8 hours) with a greater proportion of [^{123}I]MIP-1095 cleared via the hepatobiliary route when compared to [^{123}I]MIP-1072. Little uptake was detected in the brain, which exhibits high NAALADase activity (23), indicating that [^{123}I]MIP-1072 and [^{123}I]MIP-1095 do not cross the blood-brain barrier. Minimal deiodination was observed for both compounds as the thyroid contained < 1% of the total injected dose at all time points. Since mouse prostates do not express PSMA (24,25), their prostates were not included in the analysis.

The tissue distribution of the radiolabeled antibody, ProstaScint™, was compared to [^{123}I]MIP-1072 and [^{123}I]MIP-1095 (Table 2). Clearance of ProstaScint™ from blood and non-target tissues was much slower than what was observed for the small molecules. LNCaP xenograft tumor tissue continued to accumulate ProstaScint™ over time with peak accumulation of 31.4 ± 20.7 %ID/g at the 72 hr time point (the latest time point studied). Unlike [^{123}I]MIP-1072 and [^{123}I]MIP-1095, ProstaScint™ did not accumulate in kidney tissue to an appreciable extent consistent with previously reported data (15,26) despite the fact that immunohistochemistry and RT-PCR have shown PSMA to be expressed in the proximal tubules of kidney (9,27). This may be due to the fact that ProstaScint™ binds an internal epitope of PSMA (13,14) , or because of their size antibodies do not penetrate tissues well and are not filtered by glomeruli. Despite the high accumulation in the LNCaP xenograft, the widespread use of ProstaScint™ as a diagnostic imaging agent is confounded by the high accumulation in non-target tissues. This is evident in the poor tumor:blood and tumor:skeletal muscle ratios at the time points measured (Table 3). [^{123}I]MIP-1072 and [^{123}I]MIP-1095 exhibit tumor:blood and tumor:skeletal muscle ratios >100 after only a few hours, whereas the tumor:blood ratio of ProstaScint™ reached 3 only after 72 hr, the final time point of the analysis.

Consistent with the tissue distribution studies, SPECT/CT imaging at 4 hr after injection of [^{123}I]MIP-1072 and [^{123}I]MIP-1095 revealed high uptake and selectivity for PSMA expressing tissues: kidney and LNCaP tumor (Figure 2, top). Additionally, [^{123}I]MIP-1072 and [^{123}I]MIP-1095 detected PC3 PIP (PSMA +) but not PC3 flu (PSMA −) tumors by SPECT/CT at 2 hr after injection (Figure 2 bottom), indicating that the uptake is specific to PSMA and is not related to blood flow or permeability differences between cell lines. As anticipated, high uptake was also observed in the kidneys, which express PSMA.

[^{123}I]MIP-1072 and [^{123}I]MIP-1095 bind specifically to PSMA *in vivo*

To examine the specificity of targeting PSMA *in vivo*, NCr–nu/nu mice bearing either LNCaP or PC3 xenografts were co-injected with [^{123}I]MIP-1072 or [^{123}I] MIP-1095 and 50 mg/kg of the PSMA inhibitor, PMPA. Both [^{123}I]MIP-1072 and [^{123}I]MIP-1095 localized to PSMA expressing LNCaP tumors but not to the PSMA deficient PC3 tumors. In addition, binding to the LNCaP tumor xenografts and the kidneys was blocked by co-injecting the mice with 50 mg/kg PMPA (Figure 3).

Discussion

We describe here the preclinical evaluation of two novel potential radiopharmaceuticals, [^{123}I]MIP-1072 and [^{123}I]MIP-1095, that were designed to target PSMA in prostate cancer cells and tissue. PSMA is expressed in normal prostate, brain, kidney proximal tubules, and intestinal brush border membranes. Importantly, expression is dramatically upregulated in poorly differentiated, metastatic and hormone-refractory carcinomas (9) as well as after androgen deprivation therapy (28) and in lymph node metastases (29). The function of PSMA in prostate cancer is unclear, although it is reported to play a role in tumor invasiveness (30). It has been reported that increased expression of PSMA in primary prostate cancer correlates with other adverse traditional prognostic factors and independently predicts disease outcome (31,32). Numerous studies have shown its utility as a diagnostic marker and therapeutic target with a >90% prevalence in disease (9,33). Additionally, PSMA is expressed in the endothelial cells of tumor neovasculature of many solid tumors (21,27) indicating that it may have utility as a diagnostic or therapeutic molecular target in cancers other than prostate.

Several imaging modalities are currently being collectively employed for the diagnosis, staging and prognosis of prostate cancer metastases. Conventional cross-sectional imaging with CT and MRI rely on anatomical changes (lesions >1 cm) often resulting in missed lymph node metastases. Nodal enlargement due to metastases occurs relatively late in the progression of prostate cancer and therefore neither CT nor MRI are effective at detecting the often microscopic lymph node metastases. Radionuclide bone scans are commonly used for monitoring bone metastases. However, false positives are common as a result of inflammation, previous bone injuries, and arthritis, and are especially problematic in older men (34). Therefore the need exists for new methodologies of not only detecting the primary tumor, but metastatic lesions as well.

Molecular imaging, which relies on signal from a radiotracer that binds specifically to a biochemical marker on tumor cells rather than anatomical features, may provide a means to

detect both primary cancer and metastases. SPECT and positron emission tomography (PET) are two methods commonly used to provide biochemical information through molecular imaging. ^{18}F-fluorodeoxyglucose (FDG) is a glucose analogue that is readily taken up by hypermetabolic cancer cells and is an efficient means to detect many solid tumors (35–37), but is not effective in most primary prostate tumors and metastases due to the low glycolytic rate of prostate cancer (38,39). Thus, we have undertaken an effort to improve the diagnosis and staging of prostate cancer by developing molecules that target a cancer specific biochemical marker, PSMA, for imaging by conventional SPECT technology.

[^{123}I]MIP-1072 and [^{123}I]MIP-1095, were shown here to bind specifically and with high affinity to PSMA (+) LNCaP cells but not to PSMA (−) PC3 cells. Both compounds internalized in prostate cancer cells that express PSMA in a time dependent, acid insensitive manner. Since cellular internalization was demonstrated at 37 °C but not 4 °C, it is believed that it occurs via the endocytotic pathway. Recently, other PSMA-specific inhibitors (40) and antibodies (12) have been reported to be internalized through endocytosis as well. The saturation binding and NAALADase inhibition studies revealed an approximately 5-fold greater affinity of MIP-1095 over MIP-1072. This is likely a result of additional hydrophobic contacts outside of the PSMA binding pocket. The elucidation of the co-crystal structure of PSMA with both substrates and inhibitors revealed that electrostatic interactions between the carboxylic acids of the glutamic and aspartic acid residues and Arg 534/ Arg536, and Asn519 of PSMA are critical for binding (41). In addition, there is a hydrophobic pocket accessory to the active site that may be exploited in the rational design of inhibitors. This information led us to design inhibitors based on a glutamate-urea-X heterodimer structural motif where X corresponds to an alpha amino acid. These molecules contain the three carboxylic acid groups required for binding to PSMA. The urea functional group interacts with the Zn^{2+} containing active-site and the side chains of Tyr552 and His553. Substantial differences in affinity have been reported for other halogenated glutamate-urea-lysine heterodimers of this series as a consequence of the nature of the halogen and position of the halogen on the aryl ring (18). Several other glutamate-urea-X dimers with high affinity and selectivity for PSMA expressing cells and xenografts have also been described (42–48).

[^{123}I]MIP-1072 and [^{123}I]MIP-1095 exhibited peak LNCaP tumor uptake of 17.3 ± 6.3 (at 1 hr) and 34.3 ± 12.7 (at 4 hr) % ID/g, respectively. However, high uptake was also observed in the mouse kidneys, which could be blocked by the structurally unrelated PSMA inhibitor, PMPA, indicating that the uptake was mediated by specific binding to PSMA. Several reports have confirmed that PSMA is expressed in the mouse kidneys (25,49), and similar results have been demonstrated with other agents targeting PSMA (43–46). Neither compound accumulated in the brain to an appreciable extent indicating that they do not cross the blood-brain barrier and are unlikely to interfere with the physiological NAALADase activity of glutamatergic neurotransmission. In this regard, most imaging radiopharmaceuticals do not elicit pharmacological responses as the actual mass of compound administered is typically at tracer levels. In addition, although PSMA is known to be expressed in the human prostate and kidneys, a defined physiological role has yet to be

established so it is difficult to predict the effect that [^{123}I]MIP-1072 and [^{123}I]MIP-1095 may have *a priori*.

As ProstaScint is the only FDA approved imaging agent used exclusively for the detection of prostate cancer, we sought to compare the tissue distribution of [^{123}I]MIP-1072 and [^{123}I]MIP-1095 with ProstaScint™ in LNCaP bearing xenograft mice. All three compounds localized to PSMA expressing LNCaP xenografts but with very different pharmacokinetic profiles. [^{123}I]MIP-1072 is cleared more rapidly from target and non-target tissues and primarily through urinary excretion, while [^{123}I]MIP-1095 is cleared by both urinary and hepatobiliary routes. The differences in the clearance profiles do not appear to be related to metabolism as both compounds are stable in liver microsomes and blood plasma (data not shown). ProstaScint™, like most antibodies, clears from the blood very slowly with peak accumulation in the LNCaP xenograft at the latest time point studied resulting in a low tumor:background ratio and prolonged total body exposure to radiation. One other disadvantage of ProstaScint™ is that it targets the intracellular domain of PSMA (13,14), and since antibodies do not readily cross the cell membrane; it is thought that it binds only to necrotic cells of prostate tumors. More recently, however, anti-PSMA monoclonal antibodies that target an extracellular domain of PSMA, eg. J591, have entered into clinical trials (50). We have designed small molecules with affinities similar to that of ProstaScint™ and J591, but with enhanced ability to diffuse into the extravascular space and with faster blood clearance. [^{123}I]MIP-1072 and [^{123}I]MIP-1095 retain high accumulation in PSMA expressing xenografts as evident by the tissue distribution results and the SPECT/CT images. Thus, we believe radiolabeled small molecule radiopharmaceuticals that bind PSMA offer the preferred approach. Nonetheless, ProstaScint™ and J591 have validated PSMA as an excellent target for the molecular imaging of prostate cancer.

While the initial focus here is on using [^{123}I]MIP-1072 and [^{123}I]MIP-1095 for the detection of prostate cancer, it may be possible to substitute ^{123}I with ^{131}I for targeted radiotherapy of prostate cancer. ^{131}I is commonly used in the treatment of thyroid cancer as it emits high energy (606 keV) β particles capable of ablating tumors. Of course, the potential for radiotherapy will depend upon the dose to non-target tissues, in particular the kidneys, which based on the data presented here are likely to be dose limiting. PSMA has been shown by immunohistological techniques to be expressed in human kidneys (9,27). However, there is no information on the level of expression in human kidneys as compared to mouse kidneys. A Phase I clinical trial is currently underway to evaluate [^{123}I]MIP-1072 and [^{123}I]MIP-1095 in patients with metastatic prostate cancer. If the extrapolated dosimetry data from this trial implies that the radiation to non-target organs and tissues is tolerable, radiolabeling either MIP-1072 or MIP-1095 with ^{131}I could be a powerful tool in the eradication of prostate cancer; whereby patients with positive [^{123}I]MIP-1072 or [^{123}I]MIP-1095 diagnostic scans may then be treated with the same compound radiolabeled with ^{131}I.

In conclusion, there currently exists a grave unmet medical need for new imaging modalities to assist physicians in selecting appropriate treatment regimens for prostate cancer and improving patient outcomes. We believe that the widespread availability of low molecular weight radiopharmaceuticals like [^{123}I]MIP-1072 and [^{123}I]MIP-1095, which may be

capable of detecting both the primary prostate cancer as well as soft tissue and bone metastases, will not only satisfy this critical unmet need, but could alter the current paradigm for the detection and staging of prostate cancer and offer a unique opportunity to follow response to systemic therapies by non-invasive external imaging. Patient management would be significantly improved as these molecular imaging pharmaceuticals are designed to track specifically both the location and progression of prostate tumor metastases through their PSMA expression.

Acknowledgments

Grant Support: R43 EB004253-01, U24 CA92871, and R01 CA134675

References

1. Cancer Facts and Figures. American Cancer Society; 2009.
2. Hankey BF, Feuer EJ, Clegg LX, et al. Cancer surveillance series: interpreting trends in prostate cancer--part I: Evidence of the effects of screening in recent prostate cancer incidence, mortality, and survival rates. J. Natl. Cancer Inst. 1999; 91:1017–1024. [PubMed: 10379964]
3. Thompson IM, Pauler DK, Goodman PJ, et al. Prevalence of prostate cancer among men with a prostate-specific antigen level _ or _4.0 ng per milliliter. N Engl J Med. 2004; 350:2239–2246. [PubMed: 15163773]
4. Catalona WJ, Smith DS, Ratliff TL, et al. Measurement of prostate-specific antigen in serum as a screening test for prostate cancer. N Engl J Med. 1991; 324:1156–1161. [PubMed: 1707140]
5. Tricoli JV, Schoenfeldt M, Conley BA. Detection of prostate cancer and predicting progression: Current and future diagnostic markers. Clin Can Res. 2004; 10:3943–3953.
6. Stamey TA, Johnstone IM, Mcneal JE, Lu AY, Yemoto CM. Preoperative serum prostate specific antigen levels between 2 and 22 ng/ml correlate poorly with post-radical prostatectomy cancer morphology: prostate specific antigen cure rates appear constant between 2 and 9 ng/ml. J Urol. 2002; 167:103–111. [PubMed: 11743285]
7. Andriole GL, Grubb RL 3rd, Buys SS, et al. Mortality results from a randomized prostate-cancer screening trial. N Engl J Med. 2009; 360:1310–1319. [PubMed: 19297565]
8. Israeli RS, Powell CT, Fair WR, Heston WD. Molecular cloning of a complementary DNA encoding prostate-specific membrane antigen. Cancer Res. 1993; 53:227–230. [PubMed: 8417812]
9. Silver DA, Pellicer I, Fair WR, et al. Prostate-specific membrane antigen expression in normal and malignant human tissues. Clin Cancer Res. 1997; 3:81–85. [PubMed: 9815541]
10. Horoszewicz JS, Kawinski E, Murphy GP. Monoclonal antibodies to a new antigenic marker in epithelial prostatic cells and serum of prostatic cancer patients. Anticancer Res. 1987; 7:927–936. [PubMed: 2449118]
11. Pinto JT, Suffoletto BP, Bergin TM. Prostate-specific membrane antigen: a novel folate hydrolase in human prostatic carcinoma cells. Clin Cancer Res. 1996; 2:1445–1451. [PubMed: 9816319]
12. Smith-Jones PM, Vallabahajosula S, Goldsmith SJ, et al. In vitro characterization of radiolabeled monoclonal antibodies specific for the extracellular domain of prostate-specific membrane antigen. Cancer Res. 2000; 60:5237–5243. [PubMed: 11016653]
13. Troyer JK, Beckett ML, Wright GL. Location of prostate-specific membrane antigen in the LNCaP prostate carcinoma cell line. Prostate. 1997; 30:232–242. [PubMed: 9111600]
14. Troyer JK, Feng Q, Beckett ML, Wright GL. Biochemical characterization and mapping of the 7E11-C5.3 epitope of the prostate-specific membrane antigen. Urol Oncol. 1995; 1:29–37. [PubMed: 21224087]
15. Smith-Jones PM, Vallabahajosula S, Navarro V, et al. Radiolabeled monoclonal antibodies specific to the extracellular domain of prostate-specific membrane antigen: Preclinical studies in nude mice bearing LNCaP human prostate tumor. J Nucl Med. 2003; 44:610–617. [PubMed: 12679407]

16. Milowsky MI, Nanus DN, Kostakoglu L, Sheehan CE, Vallabhajosula S, Goldsmith SJ, Ross JS, Bander NH. Vascular Targeted Therapy with Anti-Prostate-Specific Membrane Antigen Monoclonal Antibody J591 in Advanced Solid Tumors. J Clin Oncol. 2007; 25:540–547. [PubMed: 17290063]
17. Vallabhajosula S, Goldsmith SJ, Kostakoglu L, Milowsky MI, Nanus DM, Bander NH. Radioimmunotherapy of prostate cancer using 90Y- and 177Lu-labeled J591 monoclonal antibodies: effect of multiple treatments on myelotoxicity. Clin Cancer Res. 2005; 11:7195–7200s.
18. Maresca KP, Hillier SM, Femia FJ, et al. A series of halogenated heterodimeric inhibitors of prostate-specific membrane antigen (PSMA) as radiolabeled probes for targeting prostate cancer. J Med Chem. 2009; 52:347–357. [PubMed: 19111054]
19. Tang H, Brown M, Ye Y, et al. Prostate targeting ligands based on N-acetylated α-linked acidic dipeptidase. Biochem Biophys Res Comm. 2003; 307:8–14. [PubMed: 12849974]
20. Cheng Y, Prusoff WH. Relationship between the inhibition constant (K1) and the concentration of inhibitor which cause 50 per cent inhibition (I50) of an enzymatic reaction. Biochem Pharmacol. 1973; 22:3099–3108. [PubMed: 4202581]
21. Chang SS, Reuter VE, Heston WD, et al. Five different anti-prostate-specific membrane antigen (PSMA) antibodies confirm PSMA expression in tumor associated neovasculature. Cancer Res. 1999; 59:3192–3198. [PubMed: 10397265]
22. Ascoli M. Internalization and degradation of receptor-bound choriogonadotropin in Leydig tumor cells. J Biol Chem. 1982; 257:13306–13311. [PubMed: 6292185]
23. Tiffany CW, Lapidus RG, Merion A, Calvin DC, Slusher BS. Characterization of the enzymatic activity of PSM: Comparison with brain NAALADase. The Prostate. 1999; 39:28–38. [PubMed: 10221263]
24. Aggarwal S, Ricklis R, Williams SA, Denmeade SR. Comparative study of PSMA expression in the prostate of mouse, dog, monkey, and human. The Prostate. 2006; 66:903–910. [PubMed: 16496413]
25. Bacich DJ, Pinto JT, Tong WP, Heston WD. Cloning, expression, genomic localization, and enzymatic activities of the mouse homolog of prostate-specific membrane antigen/NAALADase/folate hydrolase. Mamm Genome. 2001; 12:117–123. [PubMed: 11210180]
26. Lopes DA, Davis WL, Rosenstraus MJ, Uveges AJ, Gilman SC. Immunohistochemical and Pharmacokinetic Characterization of the Site-specific Immunoconjugate CYT-356 Derived from Antiprostate Monoclonal Antibody 7E11-C5. Can Res. 1990; 50:6423–6429.
27. Chang SS, O'Keefe DS, Bacich DJ, Reuter VE, Heston DW, Gaudin PB. Prostate-specific membrane antigen is produced in tumor associated neovasculature. Clin Can Res. 1999; 5:2674–2681.
28. Wright GL, Grob BM, Haley C, et al. Up-regulation of prostate-specific membrane antigen after androgen-deprivation therapy. Urology. 1996; 48:326–334. [PubMed: 8753752]
29. Sweat SD, Pacelli A, Murphy GP, Bostwick DG. Prostate-specific membrane antigen expression is greatest in prostate adenocarcinoma and lymph node metastases. J Uro.l. 1998; 52:637–640.
30. Yao V, Parwani A, Maier C, Heston WD, Bacich DJ. Moderate expression of prostate-specific membrane antigen, a tissue differentiation antigen and folate hydrolase, facilitates prostate carcinogenesis. Cancer Res. 2008; 68:9070–9077. [PubMed: 18974153]
31. Perner S, Hofer MD, Kim R, et al. Prostate-specific membrane antigen expression as a predictor of prostate cancer progression. Hum Pathol. 2007; 38:696–701. [PubMed: 17320151]
32. Marchal C, Redondo M, Padilla M, et al. Expression of prostate specific membrane antigen (PSMA) in prostatic adenocarcinoma and prostatic intraepithelial neoplasia. Histol Histopathol. 2004; 19:715–718. [PubMed: 15168332]
33. Wright GL Jr, Haley C, Beckett ML, Schellhammer PF. Expression of prostate-specific membrane antigen in normal, benign, and malignant prostate tissue. Urol Oncol. 1995; 1:18–28. [PubMed: 21224086]
34. Hricak H, Choyke PL, Eberhardt SC, Leibel SA, Scardino PT. Imaging prostate cancer: A multidisciplinary approach. Radiology. 2007; 243:28–53. [PubMed: 17392247]
35. Yamamoto T, Seino Y, Fukumoto H, et al. Over-expression of facilitative glucose transporter genes in human cancer. Biochem Biophys Res Commun. 1990; 170:223–230. [PubMed: 2372287]

36. Delbeke D. Oncological applications of FDG PET imaging. J Nucl Med. 1999; 40:1706–1715. [PubMed: 10520713]
37. Higashi K, Ueda Y, Yagishita M, et al. FDG PET measurement of the proliferative potential of non-small cell lung cancer. J Nucl Med. 2000; 41:85–92. [PubMed: 10647609]
38. Hain SF, Maisey MN. Positron emission tomography in urological tumours. BJU Int. 2003; 92:159–164. [PubMed: 12823366]
39. Shvarts O, Han KR, Seltzer M, et al. Positron emission tomography in urological cancer. Cancer Control. 2002; 9:335–342. [PubMed: 12228759]
40. Liu T, Wu LY, Kazak M, Berkman CE. Cell surface labeling and internalization by a fluorescent inhibitor of prostate-specific membrane antigen. The Prostate. 2008; 68:955–964. [PubMed: 18361407]
41. Barinka C, Byun Y, Dusich CL, et al. Interactions between human glutamate carboxypeptiase II and urea-based inhibitors:structural characterization. J Med Chem. 2008; 51:7737–7743. [PubMed: 19053759]
42. Guilarte TR, McGlothan JL, Foss CA, et al. Glutamate carboxypeptidase II levels in rodent brain using [^{125}I]DCIT quantitative autoradiography. Neurosci Lett. 2005; 387:141–144. [PubMed: 16006038]
43. Mease RC, Dusich CL, Foss CA, et al. N-[N-[(S)-1,3-dicarboxypropyl]carbamoyl]-4-[^{18}F]fluorobenzyl-L-cysteine, [^{18}F]DCFBC: A new imaging probe for prostate cancer. Clin Cancer Res. 2008; 14:3036–3043. [PubMed: 18483369]
44. Foss CA, Mease RC, Fan H, et al. Radiolabeled small-molecule ligands for prostate-specific membrane antigen: *In vivo* imaging in experimental models of prostate cancer. Clin Cancer Res. 2005; 11:4022–4028. [PubMed: 15930336]
45. Chen Y, Foss CA, Byun Y, et al. Radiohalogenated Prostate-Specific Membrane Antigen (PSMA)-Based Ureas as Imaging Agents for Prostate Cancer. J Med Chem. 2008; 51:7933–7943. [PubMed: 19053825]
46. Banerjee SR, Foss CA, Castanares M, et al. Synthesis and evaluation of technetium-99m- and rhenium-labeled inhibitors of the prostate-specific membrane antigen (PSMA). J Med Chem. 2008; 51:4504–4517. [PubMed: 18637669]
47. Kularatne SA, Wang K, Santhapuram HK, Low PS. Prostate-Specific Membrane Antigen Targeted Imaging and Therapy of Prostate Cancer Using a PSMA Inhibitor as a Homing Ligand. Mol Pharm. 2009; 6:780–789. [PubMed: 19361233]
48. Kularatne SA, Zhou Z, Yang J, Post CB, Low PS. Design, synthesis, and preclinical evaluation of prostate-specific membrane antigen targeted (99m)tc-radioimaging agents. Mol Pharm. 2009; 6:790–800. [PubMed: 19361232]
49. Gregor PD, Wolchok JD, Turaga V, et al. Induction of autoantibodies to syngeneic prostate-specific membrane antigen by xenogeneic vaccination. Int J Cancer. 2005; 116:415–421. [PubMed: 15800947]
50. Bander NH, Milowsky MI, Nanus DM, Kostakoglu L, Vallabhajosula S, Goldsmith SJ. Phase I trial of 177lutetium-labeled J591, a monoclonal antibody to prostate-specific membrane antigen, in patients with androgen-independent prostate cancer. J Clin Oncol. 2005; 23:4591–4601. [PubMed: 15837970]

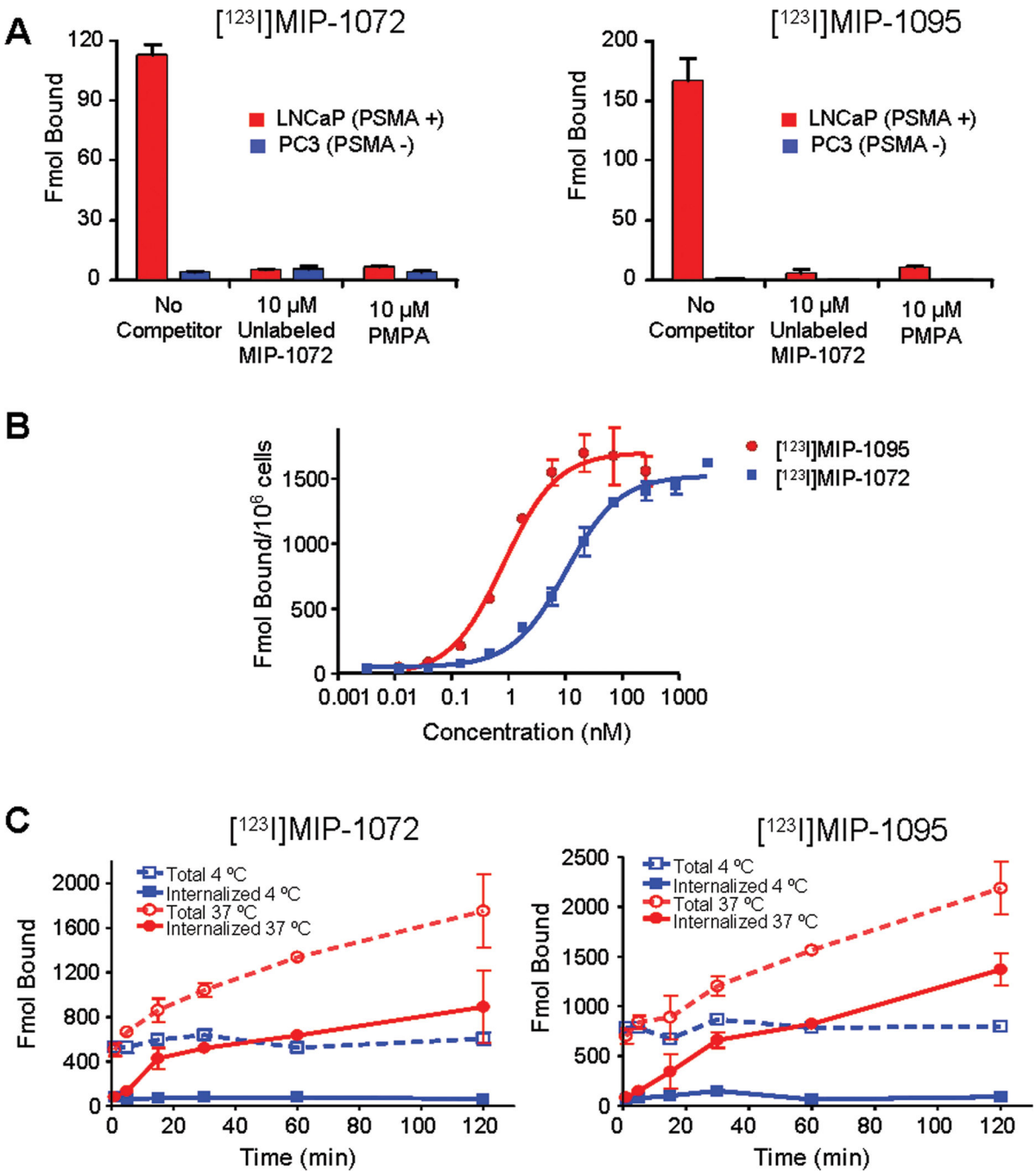

Figure 1.

A. Binding of [^{123}I]MIP-1072 or [^{123}I]MIP-1095 to LNCaP and PC3 cells. Cells were incubated for 1 hr with each compound in the absence or presence of unlabeled compound or PMPA. **B.** Saturation binding analysis of [^{123}I]MIP-1072 and [^{123}I]MIP-1095. LNCaP cells were incubated at 4 °C for 1 hr with 30–300,000 pM [^{123}I]MIP-1072 or [^{123}I]MIP-1095. The K_d and B_{max} were determined by non-linear regression analysis. **C.** LNCaP cellular internalization of [^{123}I]MIP-1072 and [^{123}I]MIP-1095. LNCaP cells were incubated with 100 nM radiolabeled compound for the indicated time, washed, and treated

with a mild acid buffer to separate cell surface bound (dashed lines) from total bound material (solid lines). The results are representative of two independent experiments.

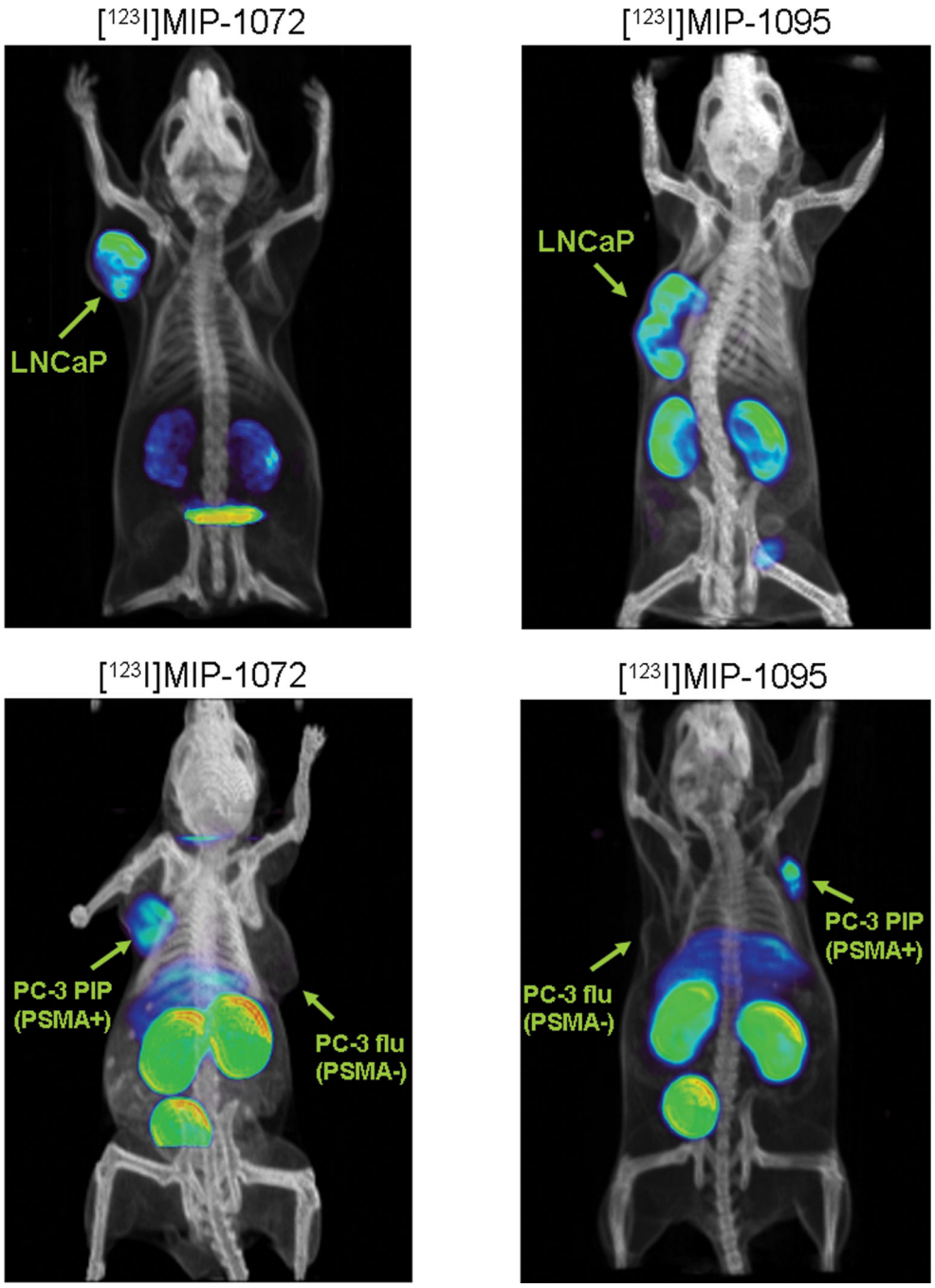

Figure 2.

Selective targeting of PSMA *in vivo* with [^{123}I]-MIP-1072 and [^{123}I]-MIP-1095. Radiolabeled compound was injected into mice bearing LNCaP xenografts and imaged by SPECT/CT at 4 hr (top) or mice bearing PC3 PIP (PSMA +) or PC3 flu (PSMA −) xenografts and imaged by SPECT/CT at 2 hr (bottom). Each mouse was injected with approximately 1 mCi of radiolabeled compound at a specific activity >1000 mCi/μmol.

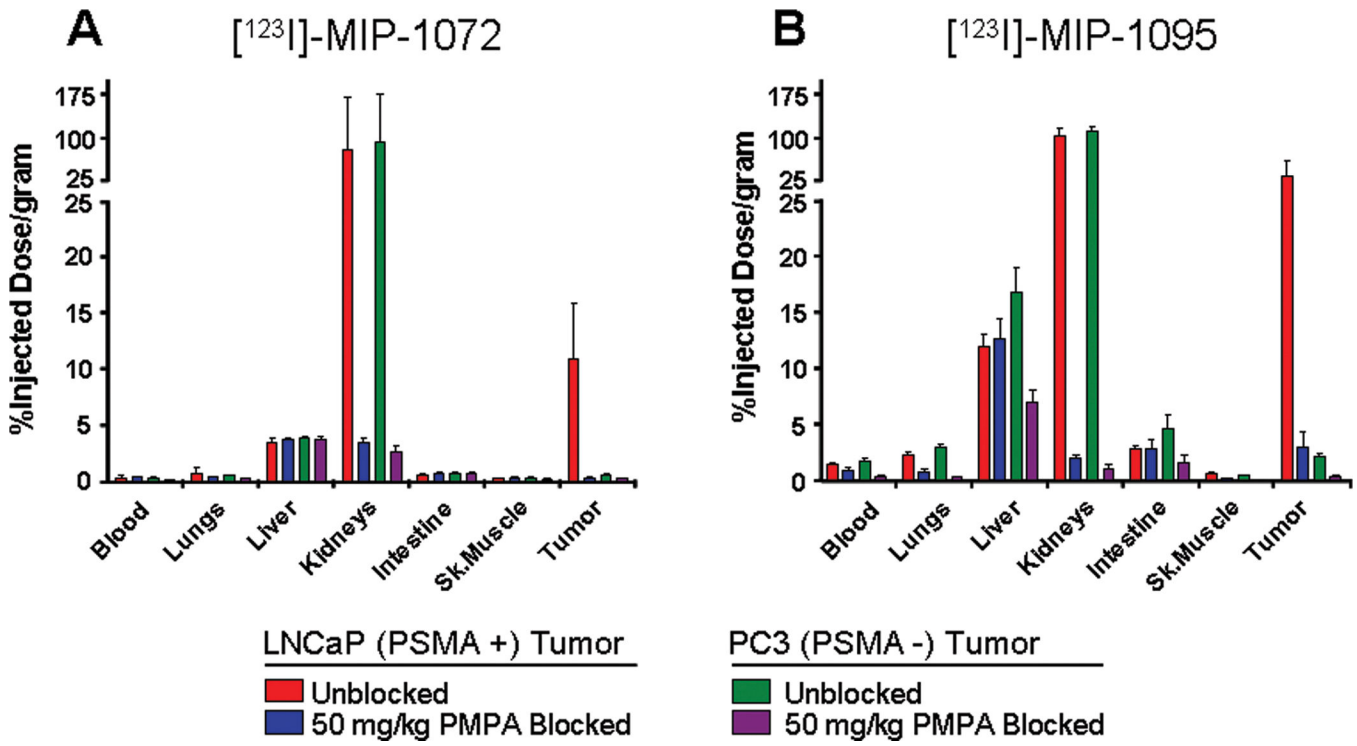

Figure 3.

Specific binding of [^{123}I]MIP-1072 (A) and [^{123}I]MIP-1095 (B) to PSMA *in vivo*. Radiolabeled compound (2 μCi/mouse at >1000 mCi/μmol) was injected alone (LNCaP tumor, PC3 tumor) or co-injected with 50 mg/kg PMPA (LNCaP tumor, or PC3 tumor) via the tail vein. Data are expressed as %ID/g.

Table 1

Tissue distribution of [^{123}I]MIP-1072 and [^{123}I]MIP-1095 in NCr nude mice bearing LNCaP xenografts.

[^{123}I]MIP-1072

	Time (hr)					
Tissue	**0.25**	**1**	**2**	**4**	**8**	**24**
Blood	2.59 ± 0.24	0.47 ± 0.15	0.21 ± 0.04	0.06 ± 0.03	0.06 ± 0.03	0.01 ± 0
Heart	1.25 ± 0.22	0.31 ± 0.08	0.19 ± 0.07	0.01 ± 0.02	0.05 ± 0.04	0.01 ± 0.05
Lungs	2.34 ± 0.61	0.86 ± 0.24	0.4 ± 0.19	0.08 ± 0.04	0.06 ± 0.03	0.05 ± 0.06
Liver	2.26 ± 0.56	2.22 ± 0.43	2.84 ± 0.63	2.17 ± 0.67	1.78 ± 0.4	0.29 ± 0.05
Spleen	4.28 ± 1.67	1.91 ± 0.85	0.75 ± 0.36	0.16 ± 0.12	0.18 ± 0.11	0.14 ± 0.1
Kidneys	90.1 ± 20.2	151 ± 26	159 ± 46	35.8 ± 18.7	21.5 ± 25.5	1.1 ± 0.6
Stomach	0.69 ± 0.17	0.26 ± 0.03	0.21 ± 0.06	0.11 ± 0.05	0.21 ± 0.08	0.11 ± 0.05
Lg Intestine	0.41 ± 0.08	0.15 ± 0.04	0.28 ± 0.12	0.48 ± 0.13	0.72 ± 0.22	0.37 ± 0.18
Sm Intestine	0.83 ± 0.1	0.41 ± 0.12	0.35 ± 0.1	0.24 ± 0.07	0.27 ± 0.06	0.07 ± 0.02
Testes	0.91 ± 0.24	0.58 ± 0.19	0.43 ± 0.16	0.26 ± 0.17	0.18 ± 0.14	0.05 ± 0.04
Sk.Muscle	0.8 ± 0.18	0.35 ± 0.17	0.2 ± 0.1	0.08 ± 0.1	0.02 ± 0.04	0.08 ± 0.04
Bone	0.69 ± 0.15	0.25 ± 0.07	0.17 ± 0.08	0.1 ± 0.18	0.04 ± 0.04	0.03 ± 0.05
Brain	0.08 ± 0.02	0.04 ± 0.01	0.04 ± 0.01	0 ± 0	0.02 ± 0.01	0.02 ± 0.01
Adipose	1.45 ± 0.27	0.74 ± 0.28	0.46 ± 0.27	0.12 ± 0.16	0.04 ± 0.11	0.01 ± 0.11
Tumor	12.9 ± 3.3	17.4 ± 6.3	14.0 ± 6.9	13.7 ± 3.1	9.74 ± 3.48	5.03 ± 1.35

[^{123}I]MIP-1095

	Time (hr)					
Tissue	**0.25**	**1**	**2**	**4**	**8**	**24**
Blood	3.75 ± 0.7	1.95 ± 0.23	1.12 ± 0.48	0.84 ± 0.23	0.49 ± 0.21	0.17 ± 0.1
Heart	2.76 ± 0.54	1.31 ± 0.22	0.78 ± 0.28	0.53 ± 0.09	0.38 ± 0.12	0.15 ± 0.08
Lungs	4.53 ± 0.66	3.22 ± 0.68	2.3 ± 1.02	1.6 ± 0.53	1.53 ± 1	0.55 ± 0.42
Liver	8.66 ± 1.54	11.3 ± 1.3	9.94 ± 2.53	7.82 ± 1.01	3.79 ± 0.87	1.31 ± 0.63
Spleen	9.65 ± 6.44	4.57 ± 0.77	3.73 ± 1.46	2.06 ± 0.63	1.34 ± 0.63	0.45 ± 0.29
Kidneys	52.2 ± 12.2	65.3 ± 7.5	88.7 ± 23.8	77.5 ± 16.6	54.8 ± 19.1	27 ± 26.2
Stomach	1.77 ± 0.52	3.02 ± 0.47	2.33 ± 1.79	4.09 ± 1.36	4.43 ± 2.28	1.15 ± 1.2

[^{123}I]MIP-1095

	Time (hr)					
Tissue	**0.25**	**1**	**2**	**4**	**8**	**24**
Lg Intestine	1.59 ± 1.45	0.87 ± 0.38	4 ± 2.82	7.55 ± 7.69	12.28 ± 5.35	4.49 ± 3.09
Sm Intestine	1.78 ± 1.05	4.4 ± 0.55	4.67 ± 0.86	6.64 ± 3.19	3.66 ± 0.9	0.76 ± 0.48
Testes	1.11 ± 0.51	0.86 ± 0.18	1.27 ± 0.31	0.84 ± 0.18	0.6 ± 0.12	0.27 ± 0.23
Sk.Muscle	0.9 ± 0.2	0.42 ± 0.03	0.34 ± 0.17	0.26 ± 0.07	0.23 ± 0.13	0.1 ± 0.04
Bone	0.9 ± 0.27	0.55 ± 0.04	0.36 ± 0.11	0.25 ± 0.04	0.28 ± 0.13	0.27 ± 0.19
Brain	0.17 ± 0.05	0.06 ± 0.03	0.06 ± 0.02	0.44 ± 0.91	0.07 ± 0.02	0.03 ± 0.01
Adipose	4.67 ± 4	2.34 ± 0.48	1.68 ± 1.15	0.86 ± 0.43	2.63 ± 4.66	0.52 ± 0.25
Tumor	7.9 ± 2.43	20.7 ± 5.8	27.3 ± 3.4	34.3 ± 12.7	28.1 ± 12.8	29.1 ± 15.1

Data are %ID/g, expressed as mean ± SD.

Table 2

Tissue distribution of ProstaScint™ in NCr nude mice bearing LNCaP xenografts.

	Time (hr)				
Tissue	**1**	**4**	**24**	**48**	**72**
Blood	30.8 ± 7.6	29 ± 5.2	15.5 ± 5	11.8 ± 0.9	10.8 ± 7.5
Heart	8.47 ± 1.17	7.87 ± 2.09	4.39 ± 1.08	2.7 ± 0.37	1.76 ± 0.36
Lungs	19.46 ± 2.65	15.07 ± 2.85	9.04 ± 2.52	6.57 ± 1.89	4.75 ± 0.73
Liver	16.7 ± 4.5	14.1 ± 2	10.2 ± 1.8	8.31 ± 1.87	7.87 ± 1.31
Spleen	9.96 ± 2.77	8.91 ± 2.44	8.61 ± 1.44	8.62 ± 1.87	8.39 ± 3.81
Kidneys	8.7 ± 1.5	8.7 ± 1.1	9 ± 1.2	9.8 ± 1	10.9 ± 3.4
Stomach	1.05 ± 0.25	1.26 ± 0.53	1.08 ± 0.41	0.82 ± 0.13	0.77 ± 0.25
Lg Intestine	0.76 ± 0.12	1.47 ± 0.34	2.68 ± 0.89	1.49 ± 0.91	1.01 ± 0.34
Sm Intestine	2.44 ± 0.5	3.23 ± 0.23	2.07 ± 0.44	1.82 ± 0.91	1.49 ± 0.29
Testes	1.73 ± 0.35	2.82 ± 0.39	1.96 ± 0.56	1.55 ± 0.2	1.45 ± 0.54
Sk.Muscle	0.85 ± 0.57	0.66 ± 0.18	0.96 ± 0.28	0.84 ± 0.08	0.76 ± 0.19
Bone	2.42 ± 0.59	2.58 ± 0.86	2.04 ± 0.47	1.64 ± 0.36	1.34 ± 0.4
Brain	0.66 ± 0.13	0.96 ± 0.69	0.38 ± 0.13	0.26 ± 0.02	0.23 ± 0.09
Adipose	2.13 ± 0.49	1.54 ± 0.71	2.16 ± 0.31	1.93 ± 0.52	1.57 ± 0.46
Tumor	3.33 ± 1.13	7.92 ± 3.17	21.8 ± 10.2	27.8 ± 10.4	31.4 ± 20.1

Data are %ID/g, expressed as mean ± SD.

Table 3

Tumor to tissue ratios of [^{123}I]MIP-1072, [^{123}I]MIP-1095, and ProstaScint™ in NCr nude mice bearing LNCaP xenografts.

		Time (hr)					
	Ratio	**0.25**	**1**	**2**	**4**	**8**	**24**
[^{123}I]MIP-1072	**Tumor:Blood**	4.97	37.1	65.4	220	176	411
	Tumor:Skeletal Muscle	16.2	50.0	70.2	182	446	64.5
[^{123}I]MIP-1095	**Tumor:Blood**	2.10	10.6	24.3	40.6	57.5	174
	Tumor:Skeletal Muscle	8.79	49.3	80.8	133	121	304

		Time (hr)				
	Ratio	**1**	**4**	**24**	**48**	**72**
ProstaScint™	**Tumor:Blood**	0.11	0.27	1.41	2.37	2.92
	Tumor:Skeletal Muscle	3.93	12.0	22.8	33.1	41.2

Data are ratios based on the %ID/g.